Particle-Specific Deflection Windows for Optical Sorting by Uncertainty Quantification

Marcel Reith-Braun[1]*, Kevin Liang[2], Florian Pfaff[1], Georg Maier[2], Robin Gruna[2], Albert Bauer[3], Harald Kruggel-Emden[3], Thomas Längle[2], Jürgen Beyerer[2], and Uwe D. Hanebeck[1]

1 Intelligent Sensor-Actuator-Systems Laboratory, Karlsruhe Institute of Technology, 76131 Karlsruhe, Germany

2 Fraunhofer IOSB, Institute of Optronics, System Technologies and Image Exploitation, 76131 Karlsruhe, Germany

3 Chair of Mechanical Process Engineering and Solids Processing, Technische Universität Berlin, 10587 Berlin, Germany

* Corresponding Author: Karlsruhe Institute of Technology, 76131 Karlsruhe, Germany, marcel.reith-braun@kit.edu

Keywords: sensor-based sorting, deflection windows, uncertainty quantification, first-passage time, constant-velocity model, constant-acceleration model

Abstract

In current state of the art sensor-based sorting systems, the length of the deflection windows, i.e., the period of nozzle activation and the number of nozzles to be activated, is commonly determined solely by the size of the particles. However, this comes at the cost of the sorting process not accounting for model discrepancies between actual and presumed particle motion, as well as for situations where the available information does not allow for precise determination of nozzle activations. To achieve a desired sorting accuracy, in practice, one is therefore usually forced to enlarge the deflection window to a certain degree, which increases the number of falsely co-deflected particles and compressed air consumption.

In this paper, we propose incorporating the uncertainty of the prediction of particle motion of *each individual particle* into the determination of the deflection windows. The method is based on the *predictive tracking* approach for optical sorting, which tracks the particles while they move toward the nozzle array based on images of an area-scan camera. Given the extracted motion information from the tracking, we propose an approximation for the distribution of arrival time and location of the particle at the nozzle array assuming nearly constant-velocity or nearly constant-acceleration particle motion behavior. By evaluating the quantile function of both distributions, we obtain a confidence interval for the arrival time and location based on prediction uncertainty, which we then combine with the particle size to form the final deflection window. We apply our method to a real sorting task using a pilot-scale chute sorter. Our results obtained from extensive sorting trials show that sorting accuracies can be remarkably improved compared with state-of-the-art industrial sorters and enhanced even further compared with predictive tracking while having the potential to reduce compressed air consumption.

1 Introduction

The aim of data processing in sensor-based sorters with pneumatic separation is essentially to determine a deflection window, i.e., to decide when, how long, and which nozzles to activate to eject a particle of an undesired class. Usually, the period of nozzle activation and the number of nozzles to be activated are determined based on the size of the respective particle (Maier et al., 2021). Therefore, although the location of the deflection window depends on the individual particle motion, its size does not. Hence, current algorithms for sensor-based sorting are unable to account for model discrepancies between actual and presumed particle motion, as well as for situations where the available information does not allow for precise determination of nozzle activations. For example, for a particle moving unusually slowly, the predicted deflection window may be too short to cover the period in which the particle passes the nozzle array, while for a particle moving strictly according to the assumed motion, it may be larger than required. This inability leads to the risk of both, particles not being ejected and falsely co-deflected particles, as well as unnecessarily high consumption of compressed air.

In practice, one is therefore usually forced to enlarge the deflection window by a fixed, often experimentally determined, amount. This amount can be viewed as an average deviation (w.r.t. all particles) or uncertainty within the forecast of particle

motion. Explicitly including such a margin is thus often essential for achieving a desired sorting accuracy. However, enlarging the deflection window comes with the drawback that in turn the number of falsely co-deflected particles as well as the compressed air consumption is increased. Given that around 70 % of the operating costs of a pneumatic sorter are attributable to compressed air generation (Gülcan & Gülsoy, 2018), larger deflection windows constitute a major cost factor, and their reduction bears enormous potential for improvement.

To address this problem, we propose incorporating the uncertainty of the prediction of particle motion of *each individual particle* into the determination of the deflection windows. The basic idea is that when the uncertainty for a particular particle is low, i.e., it is indicated that the prediction is accurate, the deflection window for that particle can be decreased, while it should be enlarged when the uncertainty is high.

Our proposed method for particle-specific deflection windows builds upon the *predictive tracking* (Maier et al., 2021; Pfaff, 2019; Pfaff et al., 2015) approach for optical sorting. While the current state of the art in the industry primarily relies on line-scan-camera-based prediction, i.e., the particles are captured by a line-scan camera shortly before they arrive at the nozzle ar-ray, predictive tracking shows significant improvements compared with line-scan-camera-based sorters (Maier, 2022; Maier et al., 2021, 2023). This is mainly because line-scan-based approaches assume a constant velocity, common to all particles, along the transport direction and zero velocity per-pendicular to the transport direction to estimate a particle's arrival time and location at the nozzle array. It therefore often fails to capture the individual particle movement correctly. Predictive tracking on the other hand uses an area-scan camera along with a multitarget tracking (MTT) algorithm to track the particles' center points while the particles are moving. In its original ver-sion, it then predicts the center points' time and location of arrival at the nozzle array based on the extracted particle-individual motion information. Since no uncertainties are considered in this step, the size of the final de-flection windows is still not dependent on the individual particle's motion, although their location is typically estimated more accurately than using a line-scan-based approach.

To incorporate uncertainties in the prediction process of predictive tracking, the key concept that we are pursuing is to derive the distributions of the particle arrival time and location at the nozzle array. These distributions explicitly encode the uncertainty inherent in the prediction, which otherwise is invisible but still present. Based on these distributions, we then find the deflection windows as the confidence intervals

for a desired confidence level , that is, we determine the deflection windows such that with probability , the particle arrives within the respective confidence interval (see Fig. 1).

From a mathematical perspective, the problem of finding the arrival time distribution of the particle center at the nozzle array can be viewed as a first-passage time problem. Here, the particle motion is described by a stochastic process, and we are interested in the distribution in the time domain that describes when the particle arrives at the nozzle array for the first time. Although first-passage time problems constitute an old and challenging class of mathematical problems, feasible approximations can be derived under some additional assumptions, as we recently proposed in (Reith-Braun, Thumm, et al., 2023). Fortunately, these assumptions are usually fulfilled by models describing particle motion in sorting tasks. For the distribution of the location of the particle's center at the nozzle array, in this paper, we propose a linearization approach for approximation of the distribution of the stochastic process describing the particle motion orthogonal to the transport direction at the first-passage time. Since it is known that incorporating particle extents into the determination of the deflection window yields better results (Maier et al., 2021; Udoudo, 2010), we then show how the above methods can be used to estimate the arrival time distributions of the particle front and back, as well as of the location of the upper and lower particle edge location during the particle's passage of the nozzle array. Finally, we show how to obtain deflection windows from these distributions using some approximations for the corresponding confidence intervals.

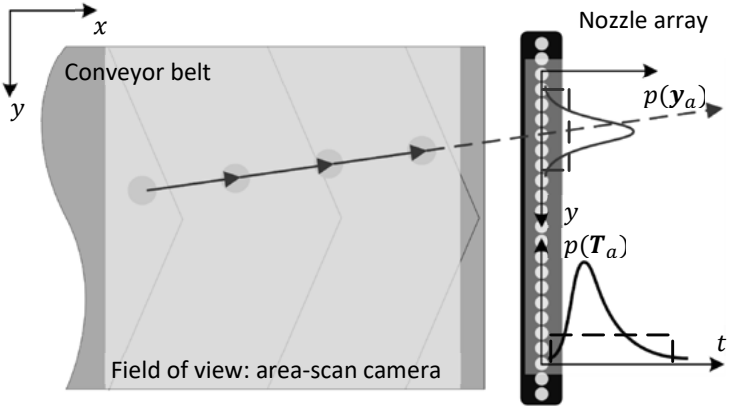

Fig. 1. Outline of our proposed method for the optical sorting problem. Particles are transported to a nozzle array (here illustrated by a conveyor belt) while being observed by an area-scan camera. We assume (nearly) constant-velocity motion behavior and track the particles with a Kalman filter. Using an estimated particle state (here the last state in the camera's field of view), we aim to estimate the distribution of the arrival time of the particle at the nozzle array (lower distribution, a distribution in the time domain) and the distribution of the particle's location (upper distribution, a distribution along the -coordinate) when passing the array of nozzles. Based on these distributions, we then calculate confidence intervals (depicted by dashed lines) used as deflection windows.

Our contributions are: First, we propose a general methodology to obtain particle-specific deflection windows based on the assumption of constant-velocity (CV) or constant-acceleration (CA) particle motion behavior. Second, we show how the distribution of the location of the particle center along the nozzle array can be approximated. Third, we propose a method to incorporate particle extents into the determination of particle-specific deflection windows and finally, we demonstrate how the parameters of the method can be determined. We evaluate our methods using numerical simulations and by applying them to a pilot-scale chute sorter in extensive sorting trials.

2 Background and Related Work

2.1 Motion Models for Describing Particle Motion

Here, we briefly describe the stochastic processes for describing particle motion that we consider in this study.

2.1.1 Constant-Velocity Model

The continuous-time (nearly) constant-velocity model, also known as the white-noise acceleration model (Bar-Shalom et al., 2001), is the Gaussian process with state $\underline{x}(t) = [x(t) \quad \dot{x}(t)]^T$, where $x(t)$ denotes the position (evolving with time t) and $\dot{x}(t)$ the velocity component, mean function

$$\underline{\hat{x}}(t) = [\hat{x}^{t_0} + \hat{\dot{x}}^{t_0}(t - t_0) \quad \hat{\dot{x}}^{t_0}] \,,$$

and covariance function $\mathrm{Cov}\{x(t)\}$ equal to

$$S \begin{bmatrix} \frac{(t-t_0)^3}{3} & \frac{(t-t_0)^2}{2} \\ \frac{(t-t_0)^2}{2} & t - t_0 \end{bmatrix} + \begin{bmatrix} \Sigma_{xx}^{t_0} + 2\Sigma_{x\dot{x}}^{t_0}(t - t_0) + \Sigma_{\dot{x}\dot{x}}^{t_0}(t - t_0)^2 & \Sigma_{x\dot{x}}^{t_0} + \Sigma_{\dot{x}\dot{x}}^{t_0}(t - t_0) \\ \Sigma_{x\dot{x}}^{t_0} + \Sigma_{\dot{x}\dot{x}}^{t_0}(t - t_0) & \Sigma_{\dot{x}\dot{x}}^{t_0} \end{bmatrix}.$$

Here, t_0 denotes the initial time, $[\hat{x}^{t_0} \quad \hat{\dot{x}}^{t_0}]^T$ is the mean of the state at t_0, and $\Sigma_{xx}^{t_0}$, $\Sigma_{x\dot{x}}^{t_0}$ and $\Sigma_{\dot{x}\dot{x}}^{t_0}$ are the respective entries of the state covariance matrix at t_0. The power spectral density S determines the amount of additional noise introduced between time t_0 and t. The CV model is linear and Markov w.r.t. the state variables. In the sense of Newtonian dynamics, the CV model has the interpretation of a freely moving particle influenced only by zero-mean white-noise random forces, with the amount of randomness controlled by S.

2.1.2 White-Noise Plus Constant Acceleration Model

The continuous-time white-noise plus constant acceleration (WN-CA) model is an extension of the CV model in which the mean function is given by

$$\underline{\hat{x}}(t) = \left[\hat{x}^{t_0} + \hat{\dot{x}}^{t_0}(t - t_0) + \frac{1}{2}a_c(t - t_0)^2 \quad \hat{\dot{x}}^{t_0} + a_c(t - t_0)\right],$$

and the state and covariance function remain the same as for the CV model. Here, a_c has the interpretation of a known, constant acceleration acting on the particle in addition to zero-mean white-noise random forces. For instance, a_c can model the

influence of gravity g in free fall ($a_c = g$) or on an inclined plane ($a_c = g \sin \alpha$, with α being the slope angle).

The discrete-time counterparts of both motion models can be obtained from the continuous-time models by fixing $\Delta t = t - t_0$ to the time difference between two consecutive time steps and treating $\underline{x}(\Delta t)$ as initial state for time step $k = 1$ and so on, i.e. $\underline{x}_{k=1} = \underline{x}(\Delta t) \mid \underline{x}^{t_0} \triangleq \underline{x}_k$, $k \in \mathbb{N}_0$, with $\underline{x}_0 = \underline{x}^{t_0}$.

2.2 Algorithms for Optical Sorting

While the current industrial state of the art is line-scan-camera-based prediction, in our previous works (Pfaff, 2019; Pfaff et al., 2015), we showed that sorting accuracy can be improved with the help of the predictive tracking paradigm. In predictive tracking, an MTT algorithm is employed on the center coordinates of the particles while they are moving. For this, an area-scan camera observes typically the last 15 to 30 cm in front of the nozzle array. In a second step, the extracted motion information is then used to precisely activate the nozzles (referred to as the prediction phase). For estimating the particle states during the MTT, multiple Kalman filters, one for each particle, using CV or CA motion models are deployed. For this, independent motion models in the transport direction, in the following referred to as the -direction, and orthogonal to the transport direction, referred to as the -direction, are used. At the end of the MTT, we are thus provided with precise estimations of the individuals particles' positions, velocities, and possibly accelerations (if a CA model is used) in the form of their expectations and covariances.

The prediction of the estimated particles' time of arrival and location at the nozzle array is then again accomplished with motion models inspired by physics, such as CV or CA models. To this end, the motion models use the expectation of the estimated particle states from the Kalman filters at the last time step before the beginning of the prediction phase. An important difference is that while in MTT, time-discrete versions of the CV or CA models are used, in the prediction of particles' time of arrival and location at the nozzle array, predictive tracking uses their time-continuous counterparts. In addition, all uncertainties are ignored, i.e., only the mean function of the time-continuous CV or CA model is used. Here, using time-continuous models allows for being independent of the camera frequency and thus being able to provide more precise nozzle activations.

Extensions to predictive tracking include incorporating orientation estimation in the MTT (Pfaff, 2019), and the use of more accurate, physically-inspired (Pfaff, 2019; Pfaff et al., 2020) and data-driven models. Latter includes the use of recurrent neural networks and multilayer perceptrons that replace the Kalman filters and the motion models as well as combinations of physically-inspired and data-driven models (Pollithy et al., 2020; Thumm et al., 2022). An experimental evaluation of some of these ideas using a lab-scale optical sorter can be found in (Maier et al., 2023). An image-based rather than a midpoint-based approach was persuaded by (Reith-Braun, Bauer, et al., 2023). Here, the sorting problem was framed as a video-forecasting task and solved using a convolutional long short-term memory network. As the approach can be trained in an unsupervised fashion, it allows sorting with a minimum of operator setup and supervision.

All algorithms eventually need to transform the information about the estimated particle arrival time and location at the nozzle array into a deflection window. This is either accomplished by targeting the particle center or, more commonly, by incorporating information about the particle extent, usually in the form of a bounding box (Maier, 2022; Maier et al., 2021; Udoudo, 2010). If the bounding box is extracted from a line-scan camera image, i.e., is in the temporal-spatial domain, it can be directly used as a deflection pattern after only minor post-processing. If the bounding box is extracted from an area-scan camera image, such as in predictive tracking, the length along the transport direction must be additionally converted to a time span by dividing by an estimated, potentially particle-dependent velocity. It is also common to use a modified version of the bounding box, e.g., by adding an offset or by multiplication with a factor. For example, an offset in -direction may account for the spatial resolution of the nozzle array (Maier et al., 2021). In general, larger deflection windows considerably improve the reliable deflection of unwanted particles. However, they also increase compressed air consumption and the number of falsely co-deflected particles. The parameters therefore need to be tuned carefully, e.g., be preliminary experiments, and a proper choice may additionally depend on the particle type (Maier, 2022; Maier et al., 2021). A scheme for determining proper parameters based on recorded particle tracks and their deviations was proposed in (Maier, 2022).

2.3 First-Passage Time Problems

The first-passage time is defined as the event $T_a = \inf\{t > t_0 : x(t) = a\}$, i.e., the first time $t > t_0$, a particle moving according to a stochastic process $x(t)$ reaches a fixed boundary $a \in \mathbb{R}$. In general, solving this problem, known as a first-passage time problem, is a challenging task, with solutions only known for very few process–boundary pairs (Blake & Lindsey, 1973; Nobile et al., 1985). An important general observation is that the event $T_a < t$ is equivalent to the event that the maximum of the process within the time range $[t_0, t)$, $m_t = \sup_{t_0 \leq s < t} x(s)$ is greater than or equal to a, i.e., $T_a < t \Leftrightarrow m_t \geq a$. Furthermore, it holds that

$$\mathbb{P}(\boldsymbol{T}_a < t) = \mathbb{P}(\boldsymbol{x}(t) > a) + \mathbb{P}(\boldsymbol{T}_a < t, \boldsymbol{x}(t) \leq a) \,, \tag{1}$$

that is, to have a first-passage time smaller than t, a particle must be either located above a at time t or, if not, must have crossed the boundary at some time $T_a < t$. However, $\mathbb{P}(T_a < t, x(t) \leq a)$ in general is intractable.

In (Reith-Braun, Thumm, et al., 2023), we proposed two methods to approximate the distribution of T_a, the first-passage time distribution (FPTD), under some additional assumptions on the process-boundary pair, such as that there is a dominant drift that causes a first-passage almost surely. These assumptions are usually fulfilled by motion models that, e.g., describe technical transport processes. The best proven method, referred to as *no-return approximation*, uses the relation (1) and additionally assumes that once a particle has crossed the boundary, it cannot return to a position smaller than a (hence, the name) – a condition that is usually satisfied in technical transport processes. Consequently, $\mathbb{P}(T_a < t, x(t) \leq a) = 0$ and $\mathbb{P}(T_a < t) = \mathbb{P}(x(t) > a)$ (for a mathematical more rigorous treatment of the above assumption and the domain in which the approximation is valid, we refer to (Reith-Braun, Thumm, et al., 2023)). Note that $x(t)$ represents the first component of the state vector $\underline{x}()$, and we are thus interested w.l.o.g. in the first-passage of the first state component w.r.t. a. An approximation of the FPTD can then be derived by differentiating the above relation w.r.t. t. Moreover, it is possible to find an expression for the quantile function analytically and to compute the moments numerically. The no-return approximation shows good alignment with Monte Carlo simulation for small and medium noise levels, i.e., high and medium signal-to-noise ratios.

3 Methodology

We now present how the required distributions for obtaining deflection windows can be approximated. The first part of the section focuses on the distribution of the particle's location at the nozzle array, whereas the second part shows how the particle extent can be included in the determination of the deflection windows.

3.1 The Distribution of the Particle Location at the Nozzle Array at the First Passage

For the distribution of the particle's center location along the nozzle array, we require the distribution of the process orthogonal to the transport direction at the time of the first passage. Therefore, we define the random variable $y_a = \{y(t) : t = T_a\}$, i.e., the -location at the first passage. Note that in addition to the uncertainties inherent to the process $y(t)$, an additional source of uncertainty is that time itself is random, with distribution given by the FPTD.

We propose a linearization approach to approximate the distribution of y_a that is valid for linear Gaussian state space models, such as the CV or CA model and their variants, referred to as *Gauß-Taylor approximation* (a similar method for approximation of the FPTD was proposed in (Reith-Braun, Thumm, et al., 2023)). For this, we first set up the motion equation $\underline{y}(T_a)$ in y-direction at T_a, using $\underline{y}(\hat{T}_a)$ with $\hat{T}_a = E\{T_a\}$ as initial state and neglecting additional noise (here, $E\{\cdot\}$ denotes the expectation operator). Subsequently, we linearize the motion equation using a first-order Taylor series expansion at $\hat{T}_a$ and $E\{\underline{y}(\hat{T}_a)\}$, and, from the linearization, calculate the approximate mean and variance for the distribution of $y(t)$ at the first passage. This results in $E\{y_a\}$ $E\{\underline{y}(\hat{T}_a)\}$ and variance

$$\mathrm{Var}\{\boldsymbol{y}_a\} \approx \left(\frac{\partial}{\partial \boldsymbol{T}_a} \boldsymbol{y}(\boldsymbol{T}_a)\Big|_{\substack{\boldsymbol{T}_a=\hat{T}_a \\ \underline{\boldsymbol{y}}(\hat{T}_a)=\mathrm{E}\{\underline{\boldsymbol{y}}(\hat{T}_a)\}}} \right)^2 \mathrm{Var}\{\boldsymbol{T}_a\}$$

$$+ \left(\nabla_{\underline{\boldsymbol{y}}(\hat{T}_a)} \boldsymbol{y}(\boldsymbol{T}_a)\Big|_{\substack{\boldsymbol{T}_a=\hat{T}_a \\ \underline{\boldsymbol{y}}(\hat{T}_a)=\mathrm{E}\{\underline{\boldsymbol{y}}(\hat{T}_a)\}}} \right)^{\mathsf{T}} \mathrm{Cov}\left\{\underline{\boldsymbol{y}}(\hat{T}_a)\right\} \left(\nabla_{\underline{\boldsymbol{y}}(\hat{T}_a)} \boldsymbol{y}(\boldsymbol{T}_a)\Big|_{\substack{\boldsymbol{T}_a=\hat{T}_a \\ \underline{\boldsymbol{y}}(\hat{T}_a)=\mathrm{E}\{\underline{\boldsymbol{y}}(\hat{T}_a)\}}} \right).$$

For instance, for the CV and the CA model, we have $\mathrm{Var}\{\mathrm{y}_a\} \approx \mathrm{Var}\{\mathrm{y}(\hat{\mathrm{T}}_a)\} + \mathrm{E}\{\dot{\mathrm{y}}(\hat{\mathrm{T}}_a)\}^2 \mathrm{Var}\{\mathrm{T}_a\}$. We then assume a Gaussian density for the distribution of the arrival location y_a.

3.2 Deflection Windows Including Particle Extents

So far, we considered the particles as point masses, i.e., they were fully described by their center points. However, for a more realistic model, we need to take the particles' extents into account. We now propose a method for including particle extents in the determination of the deflection windows.

3.2.1 Temporal Deflection Windows

We propose to determine the temporal deflection windows based on the marginal distributions of the particle front arrival time $\mathrm{T}_{(a-l/2)}$ and the particle back arrival time $\mathrm{T}_{(a+l/2)}$, where l denotes the length of the particle in transport direction. Here, we assume that l does not change much (e.g., due to rotations) while passing the nozzle array. Particle extents may be then included by solving

$$\mathbb{P}\left(\boldsymbol{T}_{a-\frac{l}{2}} < t_{\text{start}}\right) = \frac{1-q}{2}\,, \qquad \mathbb{P}\left(\boldsymbol{T}_{a+\frac{l}{2}} < t_{\text{end}}\right) = \frac{1+q}{2}$$

for t_{start} and t_{end}, respectively, where t_{start} and t_{end} describe the lower and upper bound of the time interval within which the nozzles should be open. As before, $q \in (0,1)$ denotes a desired confidence level with which one may wish to eject the particles. Solving the above equation essentially requires the quantile, or percent-point function (PPF), of the FPTD of $\mathrm{T}_{(a-l/2)}$ and $\mathrm{T}_{(a+l/2)}$, which is available for the no-return approximation.

3.2.2 Spatial Deflection Windows

For the derivation of the spatial deflection windows, i.e., the dimension of the window along the nozzle array, we introduce two new random variables, namely the upper and the lower particle edge location during the particle's passage of the nozzle array. These are defined by

$$\boldsymbol{y}_{\min} = \min\left\{\boldsymbol{y}(t) - \frac{b}{2} : \boldsymbol{T}_{a-\frac{l}{2}} < t < \boldsymbol{T}_{a+\frac{l}{2}}\right\},$$
$$\boldsymbol{y}_{\max} = \max\left\{\boldsymbol{y}(t) + \frac{b}{2} : \boldsymbol{T}_{a-\frac{l}{2}} < t < \boldsymbol{T}_{a+\frac{l}{2}}\right\}.$$

Here, b is the particle width orthogonal to the transport direction (we again assume that b, l do not change much). We then may again determine the deflection windows by solving

$$\mathbb{P}(\boldsymbol{y}_{\min} < y_{\text{low}}) = \frac{1-q}{2}, \qquad \mathbb{P}(\boldsymbol{y}_{\max} < y_{\text{up}}) = \frac{1+q}{2}$$

for y_{low} and y_{up} that describe the lower and upper bounds of the spatial deflection window. This means we require the PPFs of y_{min} and y_{max}.

However, note that deriving the distributions of y_{min} and y_{max} itself requires solving an additional first-passage time problem, due to the equivalence of maximum and first-passage time problems. For this reason, to render the problem feasible, we introduce the additional assumption that the process $y(t)$ is either monotonously increasing or monotonously decreasing in $t \in (T_{(a-l/2)}, T_{(a+l/2)})$. Incorporating this assumption yields

$$\boldsymbol{y}_{\min} = \min\left\{\boldsymbol{y}_{a-\frac{l}{2}}, \boldsymbol{y}_{a+\frac{l}{2}}\right\} - \frac{b}{2}, \qquad \boldsymbol{y}_{\max} = \max\left\{\boldsymbol{y}_{a-\frac{l}{2}}, \boldsymbol{y}_{a+\frac{l}{2}}\right\} + \frac{b}{2}.$$

Using a similar argument as for the no-return approximation, one can approximate the distribution of y_{min} and y_{max} by the lower and upper bound

$$\mathbb{P}(\boldsymbol{y}_{\min} < y_1) \geq \max\left\{\mathbb{P}\left(\boldsymbol{y}_{a+\frac{l}{2}} < y_1 + \frac{b}{2}\right), \mathbb{P}\left(\boldsymbol{y}_{a-\frac{l}{2}} < y_1 + \frac{b}{2}\right)\right\}, \qquad (2)$$

$$\mathbb{P}(\boldsymbol{y}_{\max} < y_2) \leq \min\left\{\mathbb{P}\left(\boldsymbol{y}_{a+\frac{l}{2}} < y_2 - \frac{b}{2}\right), \mathbb{P}\left(\boldsymbol{y}_{a-\frac{l}{2}} < y_2 - \frac{b}{2}\right)\right\}, \qquad (3)$$

respectively, where the distributions of $y_{a+l/2}$ and $y_{a-l/2}$ can be approximated with the method described in Sec. 3.1. The interpretation of the above formula is that, since we cannot reasonably assume that the process is either de- or increasing, one considers each case separately and decides on the one with a higher probability. However, we cannot expect that the approximations are close to the true distributions on the entire support of y_{min} and y_{max}. On the other hand, our experiments suggest that they are close to the true distribution in the technically relevant regions, i.e., for small probabilities $\mathbb{P}(y_{min} < y_1)$ and high probabilities $\mathbb{P}(y_{max} < y_2)$.

As an approximation for the PPF of y_{min} and y_{max} for small confidence levels q_1 and high confidence levels q_2, we use

$$y_1 = -\frac{b}{2} + \min\left\{y_1^1 \colon \mathbb{P}\left(\boldsymbol{y}_{a-\frac{l}{2}} < y_1^1\right) = q_1,\ y_1^2 \colon \mathbb{P}\left(\boldsymbol{y}_{a+\frac{l}{2}} < y_1^2\right) = q_1\right\},$$

$$y_2 = \frac{b}{2} + \max\left\{y_2^1 \colon \mathbb{P}\left(\boldsymbol{y}_{a-\frac{l}{2}} < y_2^1\right) = q_2,\ y_2^2 \colon \mathbb{P}\left(\boldsymbol{y}_{a+\frac{l}{2}} < y_2^2\right) = q_2\right\},$$

that is, we use the smallest value of y_1 and y_2 the highest value of that satisfy (2) and (3) since our bounds will reach q_1, q_2 after, respectively before $\mathbb{P}(y_{min} < y_1)$ and $\mathbb{P}(y_{max} < y_2)$. The PPFs, $q \to \{y\colon \mathbb{P}(y_{(a-l/2)}<y)=q\}$ and $q \to \{y\colon \mathbb{P}(y_{(a+l/2)}<y)=q\}$ can be easily approximated using the Gauß-Taylor method presented in Sec. 3.1.

4 Experimental System and Employed Algorithms

For our experiments, we use the pilot-scale optical chute sorter displayed in Fig. 2. The sorter has a chute width of 700 mm and is equipped with a Baumer VLXT-50C.I Bayer RGB area-scan camera with a maximum resolution of 2448 × 2048 pixels. The system can use transmitted light for transparent objects and reflected light for opaque objects. The resolution of the installed nozzle array is 1000 Hz in the temporal domain and approximately 5.2 mm in the spatial domain, i.e., we can activate the nozzles in discrete steps of 1 ms and each nozzle covers approximately 5.2 mm along the nozzle array.

The employed algorithm implements predictive tracking, as well as line-scan-camera-based sorting. For the latter, the line-scan camera is simulated using the area-scan camera by reducing the height of the image acquisition to a row of 1808 × 2 pixels, allowing a frame rate of 5000 fps. For predictive tracking, a frame rate of 250 fps and a resolution of 1808 × 952 pixels is used, which corresponds

to a camera field of view of approximately 628 331 mm. For tracking, a time-discrete WN-CA model is used to model the particle motion in the transport direction, while a time-discrete CV model is used for the -direction. The slope angle for the WN-CA model was 41.5°, although the chute has a slope of 55°. The difference between both accounts for friction forces acting on the particles and was determined experimentally.

The original version of predictive tracking, i.e., the version without considering prediction uncertainties for the deflection window, uses the mean function of the time-continuous WN-CA model with the same slope angle as before to determine the time of arrival and the mean function of the time-continuous CV model to determine the location of arrival. We use this version for comparison with our new method (in the remainder of the paper simply referred to as predictive tracking). In line-scan-camera-based sorting and the original version of predictive tracking, the size of a deflection window is determined based on the size and velocity of the respective particle, plus a fixed enlargement (as explained in Sec. 2.2). In our newly proposed version of predictive tracking (hereinafter referred to as *adaptive deflection*), the size of the deflection window is determined by the uncertainty of the motion prediction of the particle's front and back and uppermost and lowermost edge, as described in the previous section.

Fig. 2. Image of the sorting system. The material is fed into the system via a vibration feeder and a chute (on the right in the image). It is perceived by an area-scan camera, which is located at the top left of the image. Below the chute is an array of compressed air nozzles that separate the material.

5 Evaluation

Our evaluation consists of two parts: We first demonstrate the power of our approximation schemes by a numerical verification and then, after some parameter tuning, compare the adaptive deflection method with line-scan-based prediction and predictive tracking in sorting experiments. For both parts, we consider the pilot-scale optical chute sorter presented in the previous section (respectively, a simple, geometric model of it, for the numerical verification) and recycling glass particles having diameters in the range of 6 to 30 mm.

5.1 Numerical Verification of the Derived Distributions

We demonstrate the soundness of our approximations introduced in Sec. 3 by comparing them with Monte Carlo simulations. For this, we consider the example of a virtual particle moving perfectly according to the WN-CA model in the transport direction and according to the CV model orthogonal to the transport direction. For the state distribution used as input of our approximations and all parameters of the methods, we use the values obtained by tracking a typical particle from our sorting task and the same parameters as for the final sorting experiments.

The Monte Carlo simulation uses the discrete-time counterparts of the motion models with very small time increments. In each time step, it checks if the particle center, front, and back have already crossed the nozzle array. Likewise, the particle center, uppermost, and lowermost edge locations are recorded within the period when the particle passes the nozzle array. From this information, we then extract histograms used as (approximate) ground truth for comparison with our approximations.

The results for the approximation of the FPTD and the -position at the first arrival are displayed in Fig. 3. The approximations are generally very close to the Monte Carlo histograms, with no differences in PDF and CDF visually recognizable. For comparison, the plots also show uniform distributions corresponding to the conventional case where a point prediction (in this case from predictive tracking) is used with a window length equal to the particle length divided by an estimate of the particle velocity in the -direction or the particle width, respectively, and no additional enlargement. Note that our approximations capture the true distributions way more precisely, but at this point do not account for the particle extents.

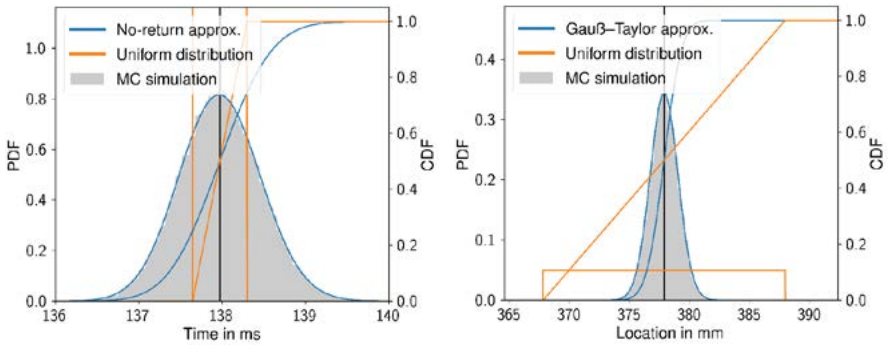

Fig. 3. The PDF and CDF of the first-arrival time distribution (left) and the distribution of the particle location along the nozzle array (right) of a typical particle from our sorting experiments. "No-return approx." denotes the similarly named approach from (Reith-Braun, Thumm, et al., 2023) for approximate FPTD. "Gauß-Taylor approx." denotes the approach proposed in Sec. 3.1 for approximation of the -location at the arrival time. "Uniform distribution" denotes the conventional approach, i.e., using a point prediction (in this case from predictive tracking, visualized by the black vertical line) for the particle arrival time and location and a window length with no additional enlargement. The shaded parts (denoted "MC simulation") display histograms of the respective distributions obtained by Monte Carlo simulations.

The results of our proposed methods for considering particle extents are visualized in Fig. 4. Again, the approximations are able to capture the true distributions for the particle under consideration with high precision. For comparison, again the same conventional approach as in Fig. 3 is displayed. Note, however, that it is here described by Dirac distributions (instead of uniform distributions), since we are now considering the particle's front and back arrival time, and its uppermost and lowermost edge location, respectively. Note that our approximation for a reasonably high always yields larger deflection windows than the ones from the conventional approach without additional enlargement, since the prediction uncertainty then adds up with the particle size. However, when the deflection windows of the conventional method are additionally enlarged, the approximation can also yield smaller deflection windows than the conventional method even if high values of are used.

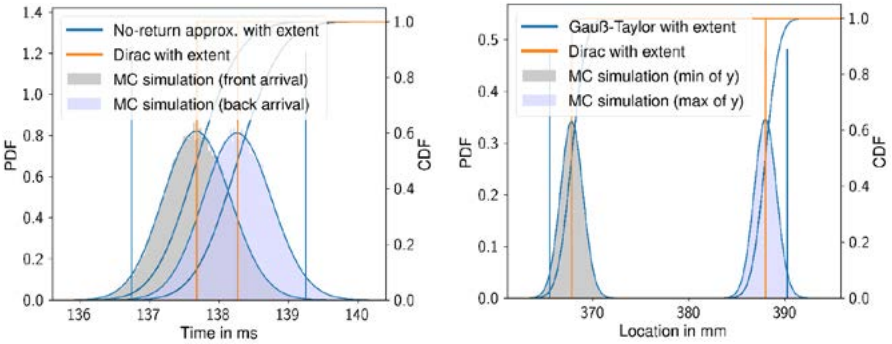

Fig. 4. The PDF and CDF of the front and back arrival time distribution (left) and the distribution of the minimum and maximum particle edge location at the nozzle array (right) of a typical particle from our sorting experiments. "No-return approx. with extents" denotes the approach described in Sec. 3.2.1. Likewise, "Gauß-Taylor with extents" denotes the approach described in Sec. 3.2.2. "Dirac with extents" denotes the usual approach, i.e., using a point prediction (in this case from predictive tracking) for the particle front and back arrival and the minimum and maximum particle edge, respectively. The shaded parts (denoted "MC simulation") display histograms of the respective distributions obtained by Monte Carlo simulations.

5.2 Sorting Experiments

The mass flow to be sorted consists of a mixture of glass recycling of 500 g white and 75 g stained glass. These particle types can be easily distinguished visually so that misclassifications can be precluded, and the sorting results are directly indicative of the effectiveness of the underlying algorithm for optical sorting. The goal of our sorting trails was to eject stained glass. The approximate mass flow during the experiments was 170 g/s. In total, we conducted five sorting trails for each of the three methods: line-scan prediction, predictive tracking, and adaptive deflection. In the following, we first describe our evaluation metrics and how we obtained the parameters of our methods, before finally presenting the sorting results.

5.2.1 Metrics

For evaluation of the sorting accuracy, we consider the true negative rate $\mathrm{TNR} = \mathrm{TN}/(\mathrm{FP} + \mathrm{TN})$ and the true positive rate $\mathrm{TPR} = \mathrm{TP}/(\mathrm{TP} + \mathrm{FN})$, where positive particles are those that should not be ejected (white glass, in our case). A high TNR thus indicates a high purity of the non-ejected fraction (there are only a few unwanted particles left), whereas a high TPR indicates a high purity of the ejected fraction (there are only a few co-deflected particles). As a measure for evaluating

the compressed air consumption, we record the nozzle time, i.e., the cumulate time for which the nozzles were opened.

5.2.2 Preliminary Sorting Experiments and Parameter Tuning

The parameters of our new approach are the power spectral densities S (in x- and y-direction) and the confidence levels q (temporal and spatial). For simplicity, we assume the same value of S in both directions. Furthermore, we use the same S for the motion models in the Kalman filters of the MTT part of predictive tracking. For the confidence levels, we chose the same $q = 0{,}95$ for all confidence intervals. Note that strictly speaking, this does not imply that we wish to eject 95 % of all unwanted particles since we apply q to the temporal and spatial deflection window independently. It remains to find a suitable value for the power spectral density S. In general, this is a difficult task. There exist multiple approaches to learning the noise from data in the literature, e.g., expectation maximization (Ghahramani & Hinton, 1996), dual (Nelson, 2000), or ensemble Kalman filtering methods (Stroud & Bengtsson, 2007), each of which has their pros and cons (see also the survey by (Zhang et al., 2016)). Yet, the choice of S has a large influence on the size of the obtained deflection widows, and therefore we require a convenient method.

Here we propose to tune S using a calibration method, i.e., we wish to choose such that 95 % of all unwanted particles appear at the nozzle array within the corresponding confidence interval. For this, we record a data set of particle tracks of the unwanted class and track the particles until they have crossed the nozzle array (for this purpose, we adjust the camera field of view, so that we can observe the nozzle array). Using the recorded tracks, we then conduct “virtual” sorting experiments, whereby we run the algorithm with a specific S and count the number of hits within the confidence interval. In this step, to obtain a more accurate estimation of the particles’ time and location of arrival at the nozzle array (respectively its front, back, and upper and lower boundary), we use a linear interpolation between the last measurement before and the first measurement after the nozzle array, similar to the concept of a virtual nozzle (see e.g., (Pfaff et al., 2015; Reith-Braun, Bauer, et al., 2023)). We then perform a line search to find the desired value of S.

To ensure a proper comparison of the approaches, we chose the length of the enlargement of the deflection windows of the line-scan and conventional predictive tracking method so that a similar nozzle time as for the adaptive deflection approach with $q = 0{,}95$ was achieved. This is to compensate for the effect that we can generally

achieve a higher TNR with a longer nozzle time. Finally, this resulted in an amount of 1.6 ms and 3.47 mm by which the deflection windows were enlarged.

5.2.3 Sorting Results

Our sorting results are visualized along with the nozzle times in Fig. 5. All three approaches yield high TNRs in the range of 90 to 100 % and high TPRs of approximately 99 % and higher. Comparing the TNR, predictive tracking achieves, as expected, on average slightly higher accuracies than line-scan-based prediction. Our new method improves on the results of predictive tracking and achieves by far the highest TNR (with an average of 96.7 %, compared with 94.6 and 94.0 % for predictive tracking and line-scan-based prediction). In addition, it also shows the lowest deviations between the different runs. Comparing the TPR, again, our new approach has the highest overall accuracy, slightly outperforming the other approaches. Looking at the cumulative activation times of the nozzles, the nozzle time is quite similar for all approaches, which indicates a proper balance within the comparison.

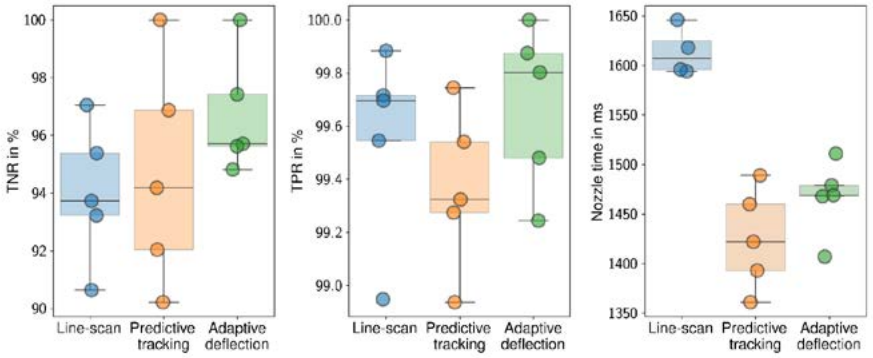

Fig. 5. Results of the sorting experiments for the three compared algorithms for optical sorting. Each point depicts the result of one of the five sorting trails. The box plots show the first, second, and third quartile of the results of the sorting trails with the whiskers extending to the most distant data point within the 1.5-fold interquartile range, starting from the upper or lower quartile, respectively.

6 Conclusion

We proposed a new method based on quantifying prediction uncertainty for determining the length of the deflection windows in optical sorting. Numerical simulations demonstrate that the approximations for the underlying distributions yield high precisions for the motion behavior of typical particles and are therefore suitable for application in optical sorters. Our sorting results show superior accuracies of the new method compared with line-scan-based prediction and predictive tracking, with an average TNR of approximately 96.7 %.

The proposed method therefore not only offers the possibility to further improve the sorting accuracy but also, and probably more importantly, to reduce the number of incorrectly deflected particles and the energy consumption by choosing the deflection window for each particle only as long as necessary. Future work may focus on this aspect, e.g., by incorporating a more accurate model of the particle–nozzle field contact and the conditions that must be satisfied for a particle to be ejected. A simple approach in this context may be to artificially reduce the size of a particle by a certain factor to account for that one may wish to target a potentially smaller range than given by the particle extent.

References

Bar-Shalom, Y., Li, X.-R., & Kirubarajan, T. (2001). Estimation with Applications to Tracking and Navigation. John Wiley & Sons, Inc.

Blake, I., & Lindsey, W. (1973). Level-crossing Problems for Random Processes. IEEE Transactions on Information Theory, 19(3), 295–315.

Ghahramani, Z., & Hinton, G. E. (1996). Parameter Estimation for Linear Dynamical Systems (CRG-TR-96-2). University of Toronto.

Gülcan, E., & Gülsoy, Ö. Y. (2018). Optical Sorting of Lignite and its Effects on Process Economics. International Journal of Coal Preparation and Utilization, 38(3), 107–126.

Maier, G. (2022). Bildfolgenbasierte Gewinnung und Nutzung partikelindividueller Bewegungsinformation in der optischen Schüttgutsortierung. KIT Scientific Publishing.

Maier, G., Pfaff, F., Pieper, C., Gruna, R., Noack, B., Kruggel-Emden, H., Längle, T., Hanebeck, U. D., Wirtz, S., Scherer, V., & Beyerer, J. (2021). Experimental Evaluation of a Novel Sensor-Based Sorting Approach Featuring Predictive Real-Time Multiobject Tracking. IEEE Transactions on Industrial Electronics, 68(2), 1548–1559.

Maier, G., Reith-Braun, M., Bauer, A., Gruna, R., Pfaff, F., Kruggel-Emden, H., Längle, T., Hanebeck, U. D., & Beyerer, J. (2023). Simulation Study and Experimental Validation of a Neural Network-based Predictive Tracking System for Sensor-based Sorting. Tm - Technisches Messen, 90(7–8), 489–499.

Nelson, A. T. (2000). Nonlinear Estimation and Modeling of Noisy Time Series by Dual Kalman Filtering Methods [PhD Thesis]. Oregon Graduate Institute of Science and Technology.

Nobile, A. G., Ricciardi, L. M., & Sacerdote, L. (1985). A Note on First-Passage Time and Some Related Problems. Journal of Applied Probability, 22(2), 346–359.

Pfaff, F. (2019). Multitarget Tracking Using Orientation Estimation for Optical Belt Sorting. KIT Scientific Publishing.

Pfaff, F., Baum, M., Noack, B., Hanebeck, U. D., Gruna, R., Längle, T., & Beyerer, J. (2015, September). TrackSort: Predictive Tracking for Sorting Uncooperative Bulk Materials. Proceedings of the 2015 IEEE International Conference on Multisensor Fusion and Integration for Intelligent Systems (MFI 2015).

Pfaff, F., Pieper, C., Maier, G., Noack, B., Gruna, R., Kruggel-Emden, H., Hanebeck, U. D., Wirtz, S., Scherer, V., Längle, T., & Beyerer, J. (2020). Predictive Tracking with Improved Motion Models for Optical Belt Sorting. At - Automatisierungstechnik, 68(4), 239–255.

Pollithy, D., Reith-Braun, M., Pfaff, F., & Hanebeck, U. D. (2020). Estimating Uncertainties of Recurrent Neural Networks in Application to Multitarget Tracking. 2020 IEEE International Conference on Multisensor Fusion and Integration for Intelligent Systems (MFI), 229–236.

Reith-Braun, M., Bauer, A., Staab, M., Pfaff, F., Maier, G., Gruna, R., Längle, T., Beyerer, J., Kruggel-Emden, H., & Hanebeck, U. D. (2023, July). GridSort: Image-based Optical Bulk Material Sorting Using Convolutional LSTMs. Proceedings of the 22nd IFAC World Congress (IFAC 2023).

Reith-Braun, M., Thumm, J., Pfaff, F., & Hanebeck, U. D. (2023, June). Approxi-mate First-Passage Time Distributions for Gaussian Motion and Transpor-tation Models. Proceedings of the 26th International Conference on In-formation Fusion (Fusion 2023).

Stroud, J. R., & Bengtsson, T. (2007). Sequential State and Variance Estimation within the Ensemble Kalman Filter. Monthly Weather Review, 135(9), 3194–3208.

Thumm, J., Reith-Braun, M., Pfaff, F., Hanebeck, U. D., Flitter, M., Maier, G., Gruna, R., Längle, T., Bauer, A., & Kruggel-Emden, H. (2022). Mixture of Experts of Neural Networks and Kalman Filters for Optical Belt Sorting. IEEE Transactions on Industrial Informatics, 18(6), 3724–3733.

Udoudo, O. B. (2010). Modelling the Efficiency of an Automated Sensor-based Sorter. Univ. Exeter.

Zhang, L., Sidoti, D., Bienkowski, A., Pattipati, K. R., Bar-Shalom, Y., & Kleinman, D. L. (2016). On the Identification of Noise Covariances and Adaptive Kal-man Filtering: A New Look at a 50 Year-old Problem. 4, 31.